Astronomy
&
Astrophysics

A Galactic Plane relative extinction map from 2MASS

D. Froebrich[1], T. P. Ray[1], G. C. Murphy[1], and A. Scholz[2]

[1] Dublin Institute for Advanced Studies, 5 Merrion Square, Dublin 2, Ireland
  e-mail: df@cp.dias.ie
[2] University of Toronto, Dept. Astronomy & Astrophysics, 66 St. George's St., Toronto, Canada

Abstract. We present three 14 400 square degree relative extinction maps of the Galactic Plane ($|b| < 20°$) obtained from 2MASS using accumulative star counts (Wolf diagrams). This method is independent of the colour of the stars and the variation of extinction with wavelength. Stars were counted in 3.5×3.5 boxes, every 20″. $1° \times 1°$ surrounding fields were chosen for reference, hence the maps represent local extinction enhancements and ignore any contribution from the ISM or very large clouds. Data reduction was performed on a Beowulf-type cluster (in approximately 120 hours). Such a cluster is ideal for this type of work as areas of the sky can be independently processed in parallel. We studied how extinction depends on wavelength in all of the high extinction regions detected and within selected dark clouds. On average a power law opacity index (β) of 1.0 to 1.8 in the NIR was deduced. The index however differed significantly from region to region and even within individual dark clouds. That said, generally it was found to be constant, or to increase, with wavelength within a particular region.

Key words. ISM: dust, extinction – infrared: ISM – methods: miscellaneous

1. Introduction

Dust is not only one of the most important coolants in molecular clouds but is also an excellent tracer of molecular hydrogen. Determining its distribution is thus crucial to understand the early stages of star formation. It gives us information, for example, on how clouds fragment and ultimately this knowledge must be reconciled with the initial mass function (Padoan et al. 1997). Moreover by combining dust extinction maps with infrared and submillimeter dust emission maps, we can derive basic knowledge of grain properties and search for evidence of grain evolution.

Extinction towards an individual star can of course by determined by measuring its colour excess although this method requires knowledge of the star's intrinsic colour (e.g. He et al. 1995; Racca et al. 2002). The technique is also highly selective as it only gives us information along very precise lines of sight. An alternative approach, developed many years ago (Wolf 1923; Bok 1956), and particularly appropriate for dark clouds, is to count the number of stars in the cloud's vicinity down to a limiting magnitude and compare this with a control "unextincted" region nearby. Such so-called Wolf Diagrams are of limited use in the optical, as one can only probe the outer peripheries of a cloud where the extinction is low. The method works well however in the infrared, due to its improved transmission with respect to the optical, allowing regions with A_V values as high as 30–40 to be measured.

Dust not only absorbs light from background stars but also reddens it. By measuring extinction in a number of wavebands, one can determine how it varies with wavelength (λ). Normally this variation is assumed to be a power law, i.e. $A_\lambda \propto \lambda^{-\beta}$ where β is the opacity index. A constant value for β however is not necessarily guaranteed a priori.

One drawback in the past of the star counting method, at least for large areas, is that it is computationally very expensive. This type of data reduction, however, is ideally suited to a parallel computing environment provided, for example, by a Beowulf-type cluster. Large swathes of the sky can be processed simultaneously and independently of each other. Moreover, the possibility for exploiting such "number crunching" facilities coincides with the availability of large ground based IR surveys such as 2MASS and DENIS. For the first time its possible to manufacture extinction maps covering large fractions of the sky.

Here we present a high spatial resolution relative extinction map of the Galactic Plane, in J, H, and K, derived from the 2MASS database using the star count method. The method and its limitations are described in detail in Sect. 2, the determination of the noise is discussed in Sect. 3. Results of the opacity index computations are presented in Sect. 4 and our conclusions are given in Sect. 5.

2. Method and limitations

Relative extinction maps were determined using Wolf diagrams (e.g. Kiss et al. 2000). At each position accumulated star counts were performed in a small box. These counts were compared to the average accumulated star count in a (co-centred but larger) comparison field to determine the relative extinction. The method is independent of stellar colour and variation of
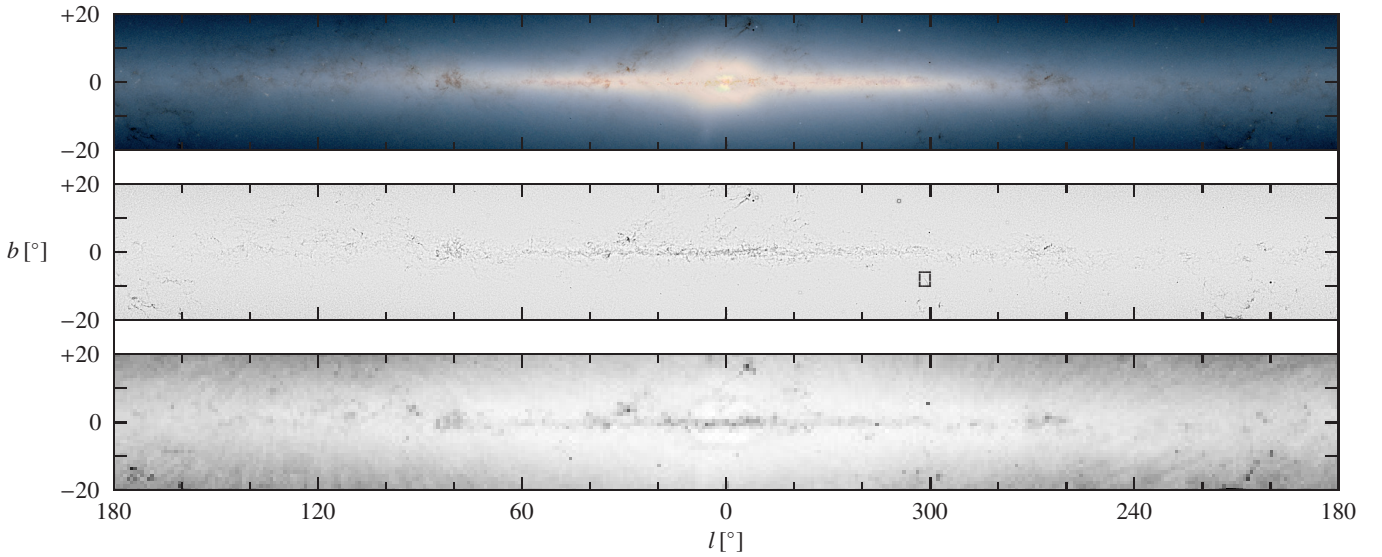
Fig. 1. *JHK* colour composite of the star count map *(top)*, relative extinction map obtained from the *J*-band data *(middle)* and three sigma noise due to the non-uniform distribution of stars in the relative extinction maps for *J (bottom)*. The noise is displayed in linear scale from zero (white) to 0.7 mag (black) of optical extinction. The rectangle marks the region magnified in Fig. 2.

extinction with wavelength. A number of assumptions, however, have to be made (e.g. Froebrich et al. 2005): (1) stars are distributed uniformly and all apparent voids are due to extinction; (2) one may define a constant average absolute magnitude for the stars in a box; (3) the completeness limit of the catalogue does not depend on position. In reality these assumptions may only be valid under certain conditions. For example reference to an average absolute magnitude is only meaningful if the box contains enough stars. Moreover stars are not distributed uniformly on the sky but if the control field is not too far away, the assumption of uniformity is locally valid. Thus, to apply the method properly one must ensure that the choice of box size, control field, etc., are within certain limits (see below).

Using the 2MASS catalogue already ensures a high level of uniformity and quality of the photometry. To avoid photometric errors for faint objects we only selected sources with a signal to noise (S/N) ratio > 5. This corresponds to quality flags A/B/C in the 2MASS catalogue, and an error in stellar magnitude of at most 0.17 mag. Such a value is slightly higher than our stepsize in brightness (counts were performed every 0.1 mag). However, the extinction is derived using an average for all stars in the box and is thus determined with greater precision.

As we have emphasised, accumulated star counts are only meaningful, providing boxes contain a sufficient number of stars. In particular the S/N in the final relative extinction maps strongly depends on the number of stars in the area being counted and hence on the box-size of the reseau (see Appendix C in Froebrich et al. 2005, for a detailed discussion). Taking into account the density of stars in the 2MASS catalogue in all 3 filters, we selected a box-size of $3\!.\!5 \times 3\!.\!5$ to perform the counts. This ensures approximately 25 stars per box ($S/N = 5$, assuming a Poisson distribution) at the completeness limit for 99.5, 73.5, 63.5% of the area with $|b| < 10°$, in J, H, and K, respectively. It also leads to a mean density of about 100 stars or more per box in the J-band for

a large area ($\approx 2800\,\square°$). Such a density converts to around one star per $20'' \times 20''$. Hence performing star counts with a spatial frequency of $20''$ ensures optimal sampling of the 2MASS catalogue. Note that this oversampling of about 10 is not unconditionally required in regions with fewer stars, but was kept to ensure a uniform pixel size throughout the whole extinction map.

Counts in the $3\!.\!5 \times 3\!.\!5$ box where compared with a co-centred larger control field. For the latter we chose a $1° \times 1°$ area. This has the effect that our maps record local extinction enhancements, due to small clouds or globules, and not global extinction effects due to the ISM or extended dark clouds.

Achieving a high S/N in our maps depends on extending the star counts to the faintest possible magnitude (and thus the largest possible number of stars). Care however has to be taken as the completeness limit of the catalogue varies strongly with galactic coordinates. We obtained this limit for each position by determining the peak in the histogram of stars per magnitude bin in the associated control field. Our relative extinction maps are then obtained exclusively using stars 0.3 mag brighter than this completeness limit.

The exercise of counting stars can be described as an embarrassingly parallel problem, as results from one part of the sky do not depend on any other. The entire 2MASS catalogue covering $|b| < 20°$ from the Galactic Plane was processed with a sampling frequency (effective pixel size) of $20''$ using our 32-node Beowulf-type cluster of 2.67 GHz P4 HyperThreat processors. The three $14\,400\,\square°$ relative extinction maps (in J, H and K) took about 40 h each to calculate.

In Fig. 1 we present a three colour composite (J, H and K) full size star count map (top panel) and the relative extinction map (middle panel) obtained from the 2MASS J-band data. The small rectangle in the figure marks the region blown-up in Fig. 2. The latter figure, of the Musca Dark Cloud,
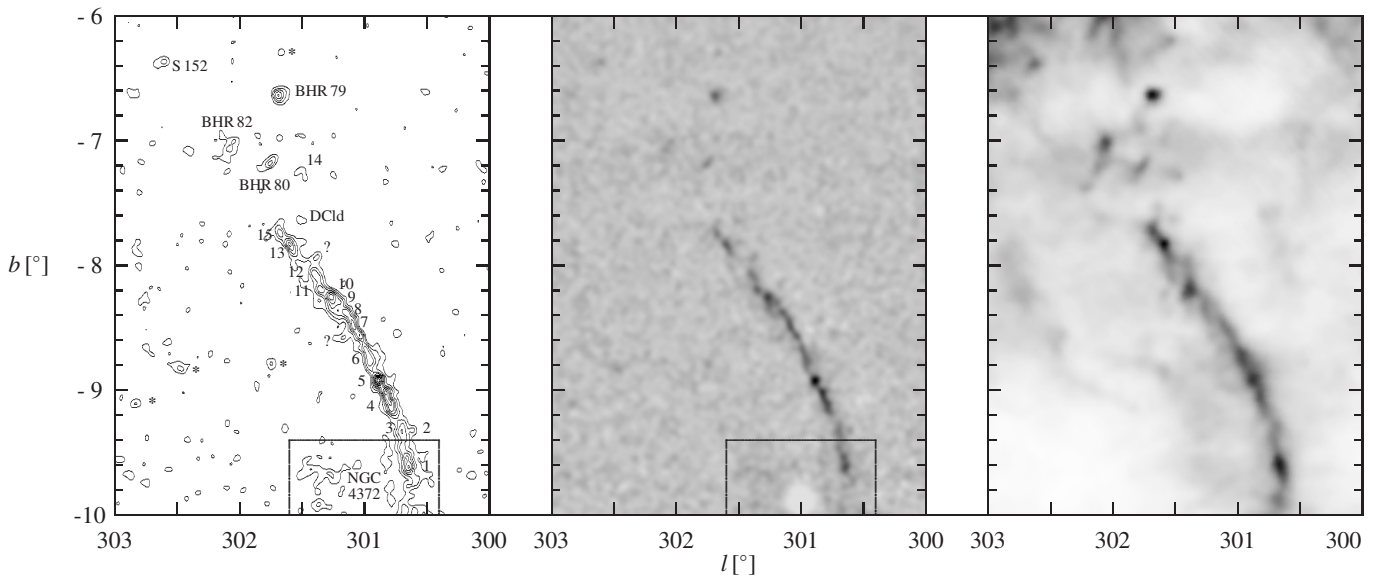
Fig. 2. Relative extinction map obtained from *J*-band 2MASS data of the Musca Dark Cloud. Contours in the *left panel* start at $A_V = 1$ mag and are in steps of 1 mag. We marked previously known and new regions with peak extinction values larger than $A_V = 2$ mag. "Fake" globules due to bright stars are labelled with *, and numbers represent regions from Vilas-Boas et al. (1994) (MU 16 could not be detected). The *middle panel* shows the relative extinction map in grey-scale and the right panel the $100\,\mu$m IRAS image of this region. In the marked rectangle, around NGC 4372, extinction values are less reliable due to additional noise (see also Sect. 2).

demonstrates the full resolution obtained in our relative extinction maps (in contours in the left and grey-scale in the middle panel). Known dark clouds are labelled, as well as "fake" globules (see below). The panel to the right of Fig. 2 shows for comparison the IRAS $100\,\mu$m image and nicely demonstrates the correspondence between dust in emission and absorption.

Comparing accumulated star counts in a $3\rlap{.}'5 \times 3\rlap{.}'5$ box with the surrounding $1° \times 1°$ field is ideal for finding small regions of enhanced extinction. All fields containing high extinction regions, which are more extended than a significant portion of one square degree, however, will not have the correct extinction values. In particular this includes the large Orion, Taurus, and Ophiuchus clouds. Here a larger comparison field is needed, but see the discussion in Sect. 4.

Very rich star clusters (mainly globular clusters) are problematic in the sense that star counts are anomalously high at their centre compared to their peripheries. This gives rise to regions of apparent negative extinction at the cluster centre and apparent positive extinction further out. Figure 2, showing the globular cluster NGC 4372, illustrates this effect. Fortunately these regions are usually not very close to areas of real higher extinction. Another effect is that extremely bright stars prevent detection of sources close by and hence also mimic high extinction regions (also see Fig. 2 for a few examples). Finally there are physical and effective gaps in the 2MASS catalogue which also result in higher apparent extinction. Fortunately these regions cover only 0.006% of the whole sky.

3. Noise determination

We determined the noise in our images to compare our method with the NICER technique of Lombardi & Alves (2001). Our relative extinction maps show noise due to the non-uniform

distribution of stars, σ_1, and the box-size within which we count stars (so-called dither noise), σ_2. The latter manifests itself as structures of around the size of the box used for star-counts. We thus smoothed the original maps with a filter of width the box-size and subtracted the resulting image from the original to obtain the noise due to the non-uniform distribution of stars. These noise images were then Gaussian filtered (5′ *FWHM*), in order to obtain the same resolution as in Lombardi & Alves (2001), and the 3σ noise level was determined. The noise is transformed into A_V using the conversion factors 4.04, 6.47, 9.75 for *J*, *H*, and *K*, respectively, given in Mathis (1990). The bottom panel in Fig. 1 shows in grayscale the resultant σ_1 noise in our *J*-band map, averaged over $1° \times 1°$.

This noise ranges from 0.2–1.0 mag (*J*), 0.4–1.8 mag (*H*), and 0.6–3.8 mag (*K*) in equivalent optical extinction. The values for the *J*-band data are slightly higher than obtained by the NICER technique (compared with the maps of Lombardi & Alves 2001, in the Orion region at about $l = 210°$, $b = -18°$). All three noise maps show the same principle structure with the lowest noise levels obtained north and south of the Galactic Plane within $\pm 60°$ longitude from the Galactic Centre. Regions directly in the Galactic Plane and within the large dark clouds (Ophiuchus, Orion, Taurus) are affected by higher noise, due to extended extinction and hence a smaller number of stars.

The additional noise, due to dithering, is only slightly dependent on the chosen box-size. A larger number of stars in the box reduces σ_2. By varying the box-size the value for this noise can be estimated. For our box-size we obtain typical values of about 0.7, 1.0, 1.3 mag optical extinction for the *J*, *H*, *K*-band dither-noise, respectively. See the Appendix of Froebrich et al. (2005) for a detailed description of this effect in the context of a particular region (IC 1396). The actual detection limit in our

relative extinction map can be determined by $\sigma_{\text{det}} = \sqrt{\sigma_1^2 + \sigma_2^2}$ for each position and filter individually.

4. NIR opacity index

Using our three large scale maps we can determine how extinction varies in the NIR. The power law index β of the wavelength dependence of the extinction can be determined using:

$$\beta_{\lambda_1 \lambda_2} = \log(A_{\lambda_1}/A_{\lambda_2})/\log(\lambda_2/\lambda_1) \tag{1}$$

where A_{λ_1} is the extinction at a wavelength λ_1. We chose the wavelength for the 2MASS filters[1] of 1.235, 1.662, and 2.159 μm for J, H, and K, respectively. Since we have three filters there are three possible combinations to determine β (JH, JK, HK), two of which are independent.

Care has to be taken in deriving β, since it is very sensitive to small errors in extinction especially at low extinction values. Hence only regions which are three sigma above the local noise level were considered. A further more complex source of error is the size and position of our control field. Due to extinction, a fraction f of the control field might just show a fraction e of stars, compared to unextincted regions. This leads to a mean extinction A_C in the control field and hence a smaller apparent measured extinction $A_\lambda = A_{\text{real}} - A_C$. It can be shown easily that under the assumptions $f \cdot (1-e) \ll 1$ and $A_C \ll A_{\text{real}}$, the derived β value is not influenced, even if the measured extinction values are wrong by A_C. The size of A_C is smaller than the noise in our maps as long as $\sqrt{N} \cdot f \cdot (1-e) \leq 1$, were N is the number of stars in our small box. According to our box-size and the star density, this holds for most regions as long as f is smaller than 0.3. Considering this we also excluded all regions where more than 30% of the control field is influenced by extinction larger than the three sigma noise from the opacity index determination.

The distribution of β_{JH}, determined over the whole area of our map is rather broad and peaks between 1.0 and 1.8. The same wide distribution is found for β_{HK}, but at slightly larger β values (shifted by $+0.1$). The reason for this particularly broad distribution can be found when we look at groups of dark clouds in detail. We find they can be categorised according to whether the opacity index 1) is roughly constant; 2) increases; or 3) decreases with wavelength in the NIR. Note that even within individual small clouds β can vary significantly. In Table 1 we list peak positions and width of the distribution of β for a selection of dark clouds. Most regions belong to Category 1 or 2, although a small number (e.g. Cepheus) can be classified as Category 3. Note that β varies significantly and ranges from 1.0 (e.g. S 140) to 2.0 (e.g. Circinus).

5. Conclusions

We have shown that accumulated star counts in the NIR can be used to obtain large scale relative extinction maps. Parallel techniques allowed us to process 14 400 square degrees of the sky within 40 h computing time on a 32-node Beowulf-type

Table 1. Peak position and width of the distribution of the opacity index β for selected dark clouds, determined between J and H (β_{JH}) and between H and K (β_{HK}). In some regions β_{HK} could not be determined properly, due to low S/N.

Region	β_{JH}	β_{HK}	Region	β_{JH}	β_{HK}
CrA	1.4 ± 0.3	1.4 ± 0.4	LupusIII	1.5 ± 0.3	1.9 ± 0.4
Ophiuchus	1.5 ± 0.3	1.7 ± 0.4	LupusIV	1.5 ± 0.3	1.9 ± 0.3
LupusI	1.5 ± 0.3	1.7 ± 0.5	Monocerus	1.4 ± 0.5	1.0 ± 0.4
LupusII	1.3 ± 0.2	–	Cepheus	1.4 ± 0.4	1.2 ± 0.4
Musca	1.7 ± 0.3	–	S140	1.0 ± 0.3	1.5 ± 0.4
Circinus	1.7 ± 0.4	2.0 ± 0.4	Serpens	1.7 ± 0.4	2.0 ± 0.3

cluster of 2.67 GHz P4 HyperThreat processors. The accumulated star counts are performed independent of stellar colour and only local extinction enhancements are determined. Hence the wavelength dependence of the dust extinction within the dark clouds can be investigated. A study of selected clouds shows that the opacity index β ranges from 1–2. In most cases a constant or increasing opacity index with wavelength is found. The large scatter of β, even within a particular cloud, leads to the conclusion that a uniform opacity index should be used with great care for extinction corrections within dark clouds. This is in contrast to the general ISM where mixing of the dust, plus averaging over long lines of sight, ensures a single index suffices.

References

Bok, B. J. 1956, AJ, 61, 309
Froebrich, D., Scholz, A., Eislöffel, J., & Murphy, G. C. 2005, A&A, 432, 575
He, L., Whittet, D. C. B., Kilkenny, D., & Spencer Jones, J. H. 1995, ApJS, 101 335
Kiss, C., Tóth, L. V., Moór, A., et al. 2000, A&A, 363, 755
Lombardi, M., & Alves, J. 2001, A&A, 377, 1023
Mathis, J. S. 1990, ARA&A, 28, 37
Padoan, P., Nordlund, A., & Jones, B. J. T. 1997, MNRAS, 288, 145
Racca, G., Gómez, M., & Kenyon, S. J. 2002, AJ, 124, 2178
Vilas-Boas, J. W. S., Myers, P. C., & Fuller, G. A. 1994, ApJ, 433, 96
Wolf, M. 1923, AN, 219, 109

---

[1] http://www.ipac.caltech.edu/2mass/releases/allsky/doc/explsup.html